Nematicity and nematic fluctuations in iron-based superconductors

Anna E. Böhmer[1,2] ✉, Jiun-Haw Chu [ID][3], Samuel Lederer[4] & Ming Yi [ID][5]

The spontaneous reduction of rotational symmetry in a crystalline solid driven by an electronic mechanism is referred to as electronic nematicity. This phenomenon—initially thought to be rare—has now been observed in an increasing number of strongly interacting systems. In particular, the ubiquitous presence of nematicity in a number of unconventional superconductors suggests its importance in developing a unified understanding of their intricate phase diagrams and superconducting pairing. In this regard, the iron-based superconductors present an ideal material platform to study electronic nematicity. Their nematic transition is pronounced, it can be studied with a wide range of experimental techniques, it is easily tunable, and high-quality samples are widely available. Signatures of nematic quantum criticality near optimal dopings have been reported in almost all families of iron-based superconductors. Here we highlight how the nematic phase in this class of materials can be addressed in its full complexity, encompassing momentum-, time-, energy- and material-dependences. We also discuss a number of important open questions that pertain to how nematicity affects the superconducting pairing and normal-state properties, and intriguing quantum-critical behaviour near the nematic transition.

'Nematicity' originally referred to a liquid-crystal phase in which rotational symmetry is broken while translational symmetry is preserved. The term was borrowed from this original context for crystalline solids, where the lowering of the discrete rotational symmetry can be spontaneously driven by electronic correlations, without breaking additional symmetries[1]. Despite its conceptual simplicity, the existence of nematicity was initially thought to be rare. Before 2008, the only systems that had been widely considered as a clean demonstration of electronic nematicity were half-filled Landau levels of a two-dimensional electron gas[2] and the field-induced phase in $Sr_3Ru_2O_7$ (ref. [3]), which was later discovered to be a spin-density wave phase[4]. The possibility of nematicity in the underdoped cuprate high-temperature superconductors was also discussed early on[5]. A major breakthrough came with the discovery of iron-based superconductors (Fe-SCs) in 2008. Similar to other high-temperature and unconventional superconductors, the high-temperature superconductivity in most Fe-SCs emerges from suppression of the parent stripe-type antiferromagnetic state[6]. However, the antiferromagnetic transition in the iron arsenides is always preceded by or coincidental with a structural transition that lowers the crystal point-group symmetry from tetragonal to orthorhombic (Fig. 1)[7]. It was soon realized that this structural transition is electronically driven[8–10]. Furthermore, in the iron chalcogenides, such as FeSe, this transition occurs without the onset of long-range magnetic order. In other words, this rotational symmetry-breaking phase transition, which is well separated from antiferromagnetism, unambiguously realizes the concept of 'nematicity' in Fe-SCs. In this Perspective we describe the current understanding of nematicity in the Fe-SCs and delineate the outstanding questions that drive the community forward.

The discovery of nematicity in Fe-SCs is important for several reasons. First, the nematic phase transition at T_{nem} is pronounced and

[1]Institute for Experimental Physics IV, Ruhr-Universität Bochum, Bochum, Germany. [2]Institute for Quantum Materials and Technologies, Karlsruhe Institute of Technology, Karlsruhe, Germany. [3]Department of Physics, University of Washington, Seattle, WA, USA. [4]University of California, Berkeley, CA, USA. [5]Department of Physics and Astronomy, Rice University, Houston, TX, USA. ✉e-mail: boehmer@physik.rub.de
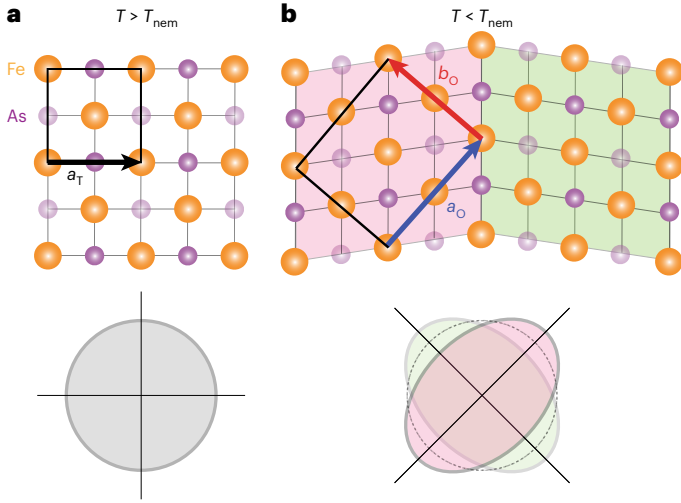
Fig. 1 | Schematic of nematicity manifested in iron-pnictide superconductors.
a, The Fe–As plane, representative of a Fe-pnictogen or Fe-chalcogen plane, in the tetragonal phase (temperature $T > T_{nem}$) with preserved C_4 symmetry (rotational symmetry schematically represented by a circle). The As atoms pucker above and below the Fe plane. The lattice constant is denoted as a_T, with the unit cell as shown. **b**, Crystal lattice in the orthorhombic phase ($T < T_{nem}$), reflecting the broken tetragonal symmetry (symmetry breaking represented by ellipses), with lattice constants a_O and b_O, and the unit cell for a nematic spin-density wave phase. Note that crystals naturally develop structural twin domains (pink and green) with opposite nematic orders. Uniaxial strain along a_O or b_O is effective at favouring one domain population over the other.

occurs at relatively high temperatures and zero magnetic field, with consequences observable over a wide energy spectrum, making it easily accessible for a variety of experimental probes. Second, the nematicity has been universally discovered in a diverse set of material families in Fe-SCs, ranging from metals with moderate correlation to strongly correlated systems on the verge of Mott localization. Third, the nematic transition temperature T_{nem} in Fe-SCs can be continuously tuned by doping and pressure, and it extrapolates to zero as the superconducting transition temperature T_c is tuned to optimal, a doping range in which signatures of nematic quantum-critical fluctuations have been observed. Finally, the strong coupling to the lattice has motivated a series of instrumental innovations that utilize the technique of stress and strain tuning. All these factors make the Fe-SCs an ideal platform with which to develop experimental and theoretical tools to explore profound concepts such as intertwined order, quantum criticality, superconductivity and non-Fermi liquid behaviour. These developments have had an impact in a wide range of quantum materials well beyond Fe-SCs.

Experimental probes of nematicity

In a system with many distinct degrees of freedom, such as a crystalline solid, nematicity manifests itself in each of them, effectively forming several nematic order parameters. To illustrate this, consider a square lattice that hosts two electronic orbitals of $[d_{xz}, d_{yz}]$ symmetry on each site. In the presence of nematic order, the crystal is deformed from square to rectangular, leading to a tetragonal to orthorhombic structural transition, the Fermi surface becomes anisotropic (with a host of consequences), the degeneracy between the d_{xz} and d_{yz} orbitals is lifted, and spin correlations become anisotropic in momentum space. These wide-ranging effects illustrate the diversity of the nematic phase and the many ways to address it.

These consequences of nematic ordering in iron-based materials are readily observed in many different experimental quantities (Fig. 2). One prominent signature is orthorhombic lattice distortion (typically on a scale of a few tenths of a percent), the occurrence of which

at a temperature greater than the magnetic ordering temperature shows that the nematic phase is distinct from the antiferromagnetic phase. The anisotropy in the electrical resistivity is prominent[11] and is probably the most studied signature of nematicity in the Fe-SCs. Other examples of nematic electronic anisotropy are found in optical properties[12], local magnetic susceptibility[13], thermoelectric properties[14] and the unidirectional electronic nanostructures around impurities[15]. In addition, a substantial anisotropy of the spin dynamics in the nematic phase, even in the absence of long-range magnetic order, has been seen using a variety of techniques[13,16,17]. Several experiments have revealed a nematic anisotropy at an unexpectedly high temperature above the bulk nematic/structural transition[18–22], which is possibly linked to defects, inhomogeneous strain or surface nematicity[23].

One particularly detailed probe of nematicity is angle-resolved photoemission spectroscopy (ARPES), which can map the change of electronic structure in the nematic phase to obtain an orbital-, momentum- and energy-resolved nematic order parameter. Polarization-sensitive measurements in both pnictide and chalcogenide materials have identified a lifting of the degeneracy between the d_{xz} and d_{yz} orbitals below T_{nem} (refs. [24,25]) in a fashion that varies strongly in different parts of the Brillouin zone[26–28]. A simple ferro-orbital order associated with an on-site energy difference translates into an energy difference between the d_{xz} and d_{yz} orbitals, independent of momentum. Therefore, the fact that the momentum-dependence of the orbital splitting is much larger than its average implies that the dominant form of the nematic order parameter must take a form beyond a simple ferro-orbital order, such as anisotropic hopping to neighbouring sites. Recently, the experimental observation of the disappearance of the d_{xz} electron pocket in the nematic phase of FeSe led to the realization that the nematic order must involve two components: both an anisotropy between the d_{xz} and d_{yz} orbitals and a rotational symmetry-breaking in the anisotropic hopping in the d_{xy} orbital[29–31]. The energy scale of symmetry breaking observed in the orbitals reflected in the energy shift of band dispersions (measured by ARPES near the Brillouin-zone corner) ranges from tens to 100 meV, which is a substantial proportion of the electronic bandwidth of most Fe-SCs, and also scales with T_{nem} (ref. [32]).

These results paint the picture of a complex and highly anisotropic electronic state coupled to a small and relatively simple lattice distortion. This opens up the technological possibility of accessing and controlling the nematic state using uniaxial stress or strain. For example, uniaxial stress can be used to solve the practical issue of 'twinning', meaning the formation of spatial domains with opposite sign of the nematic order parameter below the nematic transition (Fig. 1), and enables the measurement of nematic anisotropy with macroscopic probes[11,33]. In addition, anisotropic strain in the proper symmetry channel couples bilinearly to the electronic nematic order parameter. Thus, such a strain component can be seen as the conjugate field to the electronic nematic order parameter in a Landau framework, and one may define the nematic susceptibility as the strain-derivative of the nematic order parameter, which opens up new experimental avenues to probe nematicity (Fig. 2). Note that the bare nematic susceptibility, χ_{nem}, is frequently used; this relates to the nematic order as if it were decoupled from the lattice. χ_{nem} is enhanced but finite at T_{nem}, diverging towards a temperature $T_0 < T_{nem}$. However, χ_{nem} is renormalized by electron–lattice coupling, and the true nematic susceptibility naturally diverges at T_{nem}.

The application of controlled strain removes the lattice as an active player and, therefore, the ratio of induced electronic anisotropy to applied anisotropic strain can be taken as a measure of the bare nematic susceptibility[10]. Figure 2 highlights various typical results along these lines. The resistivity develops an in-plane anisotropy when a sample is subjected to strain in the appropriate symmetry channel. Taking the resistivity anisotropy as a measure of nematic order, the corresponding elastoresistivity coefficient (Fig. 2a) thus becomes a measure of the nematic susceptibility, with a proportional constant that encodes
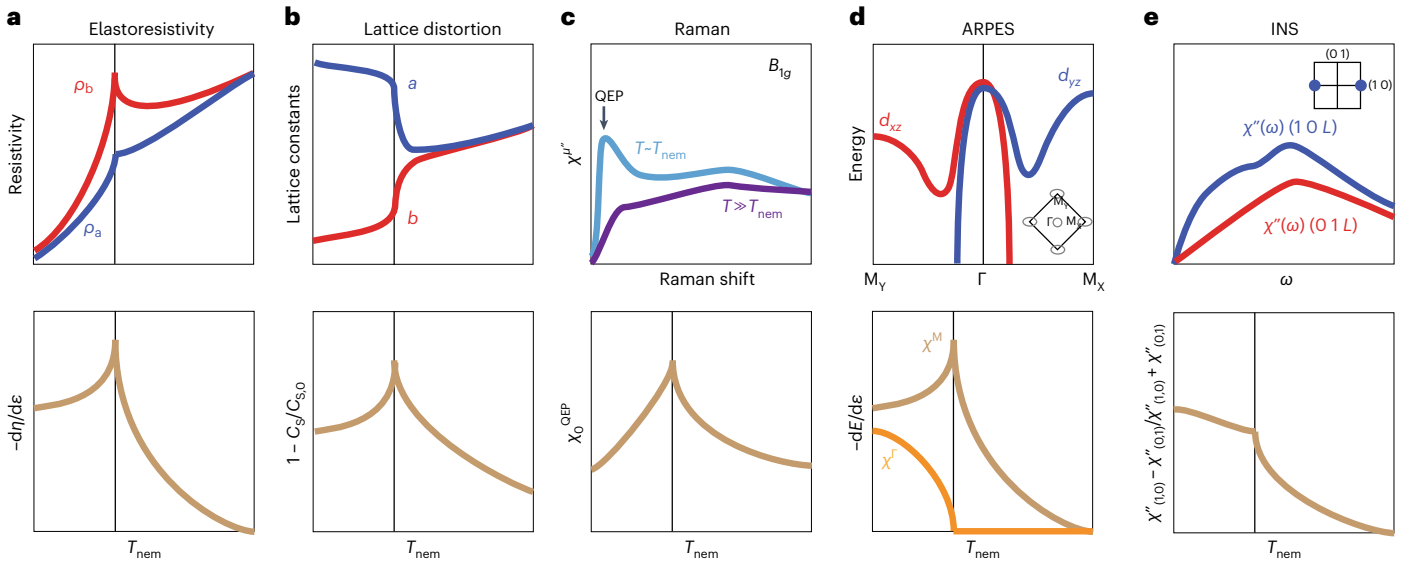
Fig. 2 | Signatures of nematicity in experimental probes. The upper panels present the experimental quantities and the lower panels mainly the derived nematic susceptibility. ε represents the strain in the nematic symmetry channel. **a**, Elastoresistivity measures the resistivity (ρ) difference along the orthorhombic axes, $\eta = (\rho_a - \rho_b)/(\rho_a + \rho_b)$. Nematic susceptibility can be extracted from tunable strain measurements[10]. **b**, The nematic lattice distortion can also be determined from dilatometry measurements of the changes in the lattice parameters a and b, and the nematic susceptibility from the renormalization of the corresponding shear modulus $C_s/C_{s,0}$ (ref. [35]). **c**, Electronic Raman spectroscopy can directly measure the nematic susceptibility in the B_{1g} channel defined in the 1-Fe unit cell, where the emergence of a quasi-elastic peak (QEP) is observed close to T_{nem}. Static nematic susceptibility (χ_0^{QEP}) can be obtained by Kramers–Kronig transformation of the Raman response function[91]. **d**, ARPES measurements show an anisotropic shift between the d_{xz} and d_{yz} dominated dispersions along orthogonal directions. The energy difference (E) as a function of tunable strain can also be used to obtain momentum-dependent nematic susceptibility[38]. **e**, INS reveals anisotropy in the spin excitations between the $(HKL) = (1, 0, L)$ and $(0, 1, L)$ directions[16]. Note that a divergent nematic susceptibility is observed by all probes shown here, except that plotted for the INS, which plots the anisotropy of the momentum- and frequency-dependent magnetic susceptibility, $\chi''(q, \omega)$, as a function of temperature.

nemato-transport coupling details[34]. Although the in-plane lattice constants naturally differ in the nematic (and orthorhombic) phase, the corresponding shear modulus (Fig. 2b) is linked to the nematic susceptibility, because a propensity to form nematic order reduces the cost of an orthorhombic lattice distortion[8,35]. This thermodynamic quantity furthermore allows to connect the 'bare' and 'true' nematic susceptibilities in a straightforward manner[36]. A special role is played by the electronic Raman response function (Fig. 2c). It probes charge fluctuations in specific symmetry channels, so it can be used to determine the nematic susceptibility without application of external strain[37]. ARPES measurements (Fig. 2d) show the anisotropic shift between the d_{xz} and d_{yz} dominated dispersions along orthogonal directions. The energy difference (E) as a function of tunable strain can also be used to obtain momentum-dependent nematic susceptibility[38]. Finally, inelastic neutron scattering (INS; Fig. 2e) reveals anisotropy in the spin excitations and the growing anisotropy of the magnetic susceptibility on approaching the nematic phase. Through continuing technological development driven by the investigation of nematic susceptiblity, a wide variety of experimental techniques can now be performed under continuously tunable strain[28,39–43].

Overall, the temperature dependence of the nematic susceptibility deduced from different probes typically agrees quite well (Fig. 2). In many systems, it can be well-approximated by a Curie–Weiss law diverging at a Weiss temperature of $T_0 < T_{nem}$ (ref. [34]), where the difference $T_{nem} - T_0$ is a measure of the corresponding nemato-elastic coupling energy. $T_{nem} - T_0$ barely varies with doping in many systems (Fig. 3c). Interestingly, the Curie constant measured by elastoresistivity shows a strong doping dependence, increasing dramatically near optimal doping in many systems (Fig. 3b)[10,34,44,45]. This is not observed by other techniques, suggesting that the nemato-transport coupling is anomalously enhanced near the quantum critical point located close to the centre of the superconducting dome.

Phase diagrams, quantum criticality and superconductivity

The Fe-SCs exhibit a stunning material diversity. They are typically classified according to their stoichiometry. However, one might also classify them according to the way that the nematic phase interacts with other phases in their composition–temperature (or pressure–temperature) phase diagrams (Fig. 3a). In the phase diagrams of most iron-pnictide compounds, the nematic order appears to be a precursor and coupled to stripe-type magnetism. In stripe-type magnetism, spins align ferromagnetically along one direction and antiferromagnetically along the orthogonal direction. Hence, in addition to rotational symmetry, both time-reversal and translational symmetries are broken. This coupling is strong for $BaFe_2As_2$, where nematicity onsets together with magnetism, and remains strong when doping occurs outside the Fe plane, such as in $BaFe_2(As,P)_2$ and all hole-doped 122-systems, such as $(Ba,K)Fe_2As_2$. In most electron-doped 122-type systems, such as $Ba(Fe,Co)_2As_2$, the coupling appears to be weakened and nematic order precedes stripe-type antiferromagnetism by a few kelvins. In the 1111- and 111-systems such as LaFeAsO and Na(Fe,Co)As, nematic order is stable in a fairly large temperature range of 20–40 K above the magnetic order, with two distinct doping-induced critical points at $T = 0$ (ref. [41]). The iron-chalcogenide system Fe(Te,Se,S) displays the largest extent of the nematic phase without long-range magnetism, centred at FeSe with a maximum ordering temperature of 90 K that is gradually suppressed by isovalent substitution on either side. Magnetic order associated with this nematic phase emerges in Fe(Te,Se,S) only under the application of hydrostatic pressure, with an unknown nature that is suspected to be stripe-type.

Despite these differences, a striking feature universally observed among different material families is the prevalence of nematic fluctuations. In $Ba(Fe,Co)_2As_2$, LaFeAsO, Fe(Se,S) and Fe(Se,Te), diverging elastoresistivity was found in a wide doping range, extending well to the
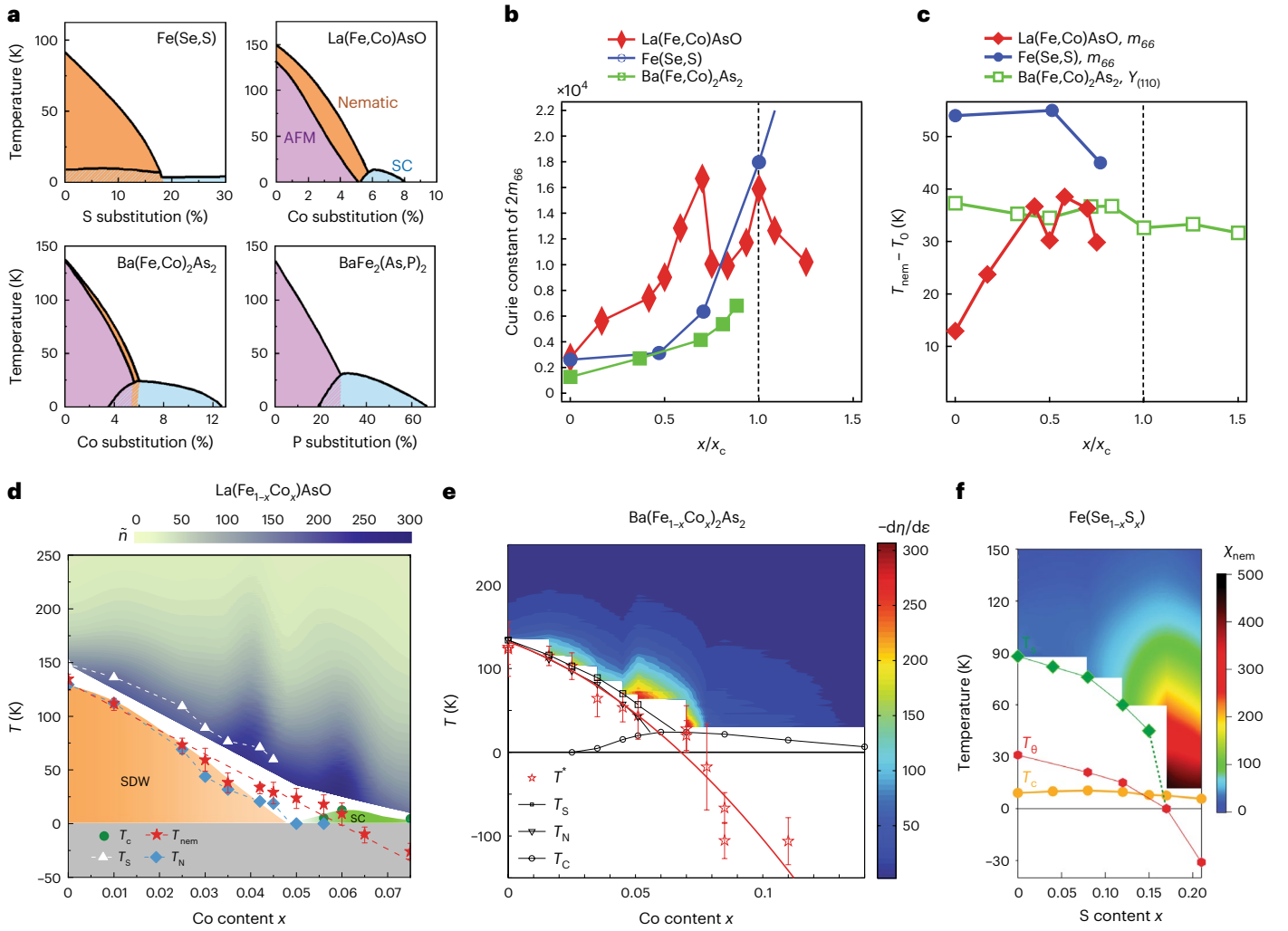
Fig. 3 | Nematic susceptibility and material diversity. a, Diversity of phase diagrams in the Fe-SCs. Common phases include the nematic phase (orange), the collinear antiferromagnetic phase (AFM, purple) and superconductivity (SC, blue). **b**, Curie constants extracted from elastoresistivity m_{66} for three representative material families, showing a rapid increase as doping x approaches the nematic critical point (x_c). Data from refs. [10,44,45]. **c**, Evolution of the measured nemato-elastic coupling in the three material families. Data from refs. [35,44,45]. **d**, Elastoresistivity $\tilde{n}$ as a measure of the nematic susceptibility in La(Fe,Co)AsO. T_S (T_N) refers to the nematic (antiferromagnetic) transition, here, and SDW stands for the stripe-type antiferromagnetic (spin-density wave) phase. **e**, Nematic susceptibility measured in Ba(Fe,Co)$_2$As$_2$. The Weiss temperature T^* crosses zero around optimal doping (red line). **f**, Nematic susceptibility measured in Fe(Se,S). The nematic transition temperature (green diamonds) extrapolates to zero around 16% S content. The error bars of the phase transition markers in **d,e** come from varying the fitting temperature range. Panels adapted with permission from: **d**, ref. [45], APS; **e**, ref. [10], AAAS; **f**, ref. [44], PNAS.

overdoped regime of the phase diagram (Fig. 3d–f)[10,34,44–46]. In each of these, with the exception of Fe(Se,S), the extracted Weiss temperature approximately reaches zero at the doping concentration with optimal T_c, suggesting the existence of a nematic quantum critical point within the centre of the superconducting dome. Similar observations were made by other experimental probes such as elastic shear modulus and electronic Raman measurements[35,37], as well as direct strain tuning[47]. The growing evidence for a nematic quantum critical point in the phase diagrams of various families of Fe-SCs raises exciting possibilities from the perspective of theory. At such a critical point, nematic fluctuations diverge in both amplitude and correlation length, making the electronic interactions they mediate both strong and long-range. Interactions mediated by such fluctuations lead to the breakdown of conventional metallic (so-called Fermi liquid) behaviour[48], and could lead to one of two possible outcomes: superconductivity or non-Fermi-liquid metallic behaviour. With respect to superconductivity, interactions mediated by near-critical nematic fluctuations are attractive in all pairing chan-nels, and can therefore enhance any pairing tendencies arising from

other interactions[49], or give rise to superconductivity on their own[49–55]. This may rationalize the near-coincidence of optimal doping and the doping of maximal nematic susceptibility in most, although not all, Fe-SCs. On the other hand, if the system remains metallic, it will develop anomalous, non-Fermi-liquid phenomenology[48,56–61]. Here, electronic excitations on the entire Fermi surface (with the possible exception of discrete points known as cold spots) become overdamped, leading to anomalous behaviour in thermodynamic probes (such as the effective mass measured in specific heat), transport (such as the temperature dependence of resistivity) and various spectroscopies. Remarkably enough, measurements in BaFe$_2$(As,P)$_2$ (refs. [62,63]) (and possibly in Fe(Se,S); ref. [64]) are consistent with this phenomenology.

Unresolved questions

The study of nematicity in iron-based systems has now entered its second decade. The community has achieved substantial progress on both experimental and theoretical fronts, with increasingly fruitful connections between the two. Having established nematicity as a central

degree of freedom, and having characterized the nematic properties in the various families of Fe-SCs, we can now address more complex and fundamental questions. These efforts will benefit tremendously from recent technological progress, particularly in strain-tuning techniques. Using strain in different symmetries as a tuning parameter or a conjugate field to nematicity, we can finally take full advantage of more sophisticated momentum-resolved[28], energy-resolved[30] and time-resolved[65] probes. Building on the current state of the art, we can identify a list of questions for the future:

(1) What is the driving mechanism of nematicity? Even though the wide-ranging effects of nematic order make it fundamentally ill-defined to speak of 'the' primary order parameter, it is nonetheless of great microscopic salience to investigate its underlying mechanism. A widely accepted view is that the nematicity in Fe-SCs can be considered a 'vestigial' order parameter resulting from the partial melting of collinear antiferromagnetism[66]. Whereas this is a natural hypothesis for the pnictides, where nematicity is always in the vicinity of antiferromagnetism, it might not be applicable to the chalcogenides, which show no long-range magnetic order at ambient pressure, and prominent spin fluctuations only deep in the nematic phase[67–69]. Alternatively, orbital order and orbital nematic scenarios have also been proposed for the chalcogenides and pnictides, where the charge and orbital channels, rather than the spin channel, break the C_4 symmetry[70,71]. However, recent ARPES results make it clear that the nematic order parameter has a prominent orbital- and momentum-dependence and that a description with a simple model, such as an on-site orbital splitting, is insufficient. Constructing a universal framework that captures the intricate interplay between the orbitals and spins in different material families remains an open challenge.

(2) How do nematicity and nematic fluctuations influence charge transport in the metallic phase? Although the resistivity anisotropy of detwinned crystals is arguably the clearest electronic manifestation of nematic order in the Fe-SCs, there is no consensus regarding its origin. There exists evidence for several theoretical propositions, including scattering from anisotropic disorder[72], scattering from anisotropic spin fluctuations[73], and anisotropic Fermi surfaces[74]. Understanding these mechanisms may help us answer a practical question: can we treat resistivity anisotropy as a faithful representation of the nematic order parameter? Perhaps more importantly, it will also shed light on the anomalous transport behaviour near the quantum critical point, such as the T-linear resistivity and enhanced Curie constant of elastoresistivity[42,75]. Correlating other measures of nematic order at different energy scales and combining with precise strain tuning and systematic doping studies is a promising line of research to investigate this question[28,76–78].

(3) How does nematicity influence the superconductivity? There are clear signs of interaction between superconductivity and nematicity[79]. Nematicity strongly competes with superconductivity in the iron pnictides, where the phase boundary is bent back within the superconducting dome[9]. Surprisingly, in Fe(Se,S), nematic order is not suppressed below T_c and appears to be enhanced instead[80]. Scanning tunnelling microscopy and ARPES studies on FeSe reveal a strongly anisotropic superconducting gap that has been understood so far as pairing primarily between electrons in the d_{yz} orbitals[81]. This result is consistent with neutron scattering reports identifying a spin resonance only where scattering along the d_{yz} channel is available. Recent studies suggest that there appear to be multiple superconducting domes in the combined phase diagrams of Fe(Se,S) and Fe(Se,Te)[46], where the superconducting gap structure undergoes an abrupt change across the nematic critical point in Fe(Se,S)[82]. Clearly, a universal

understanding of the coupling between nematicity and superconducting pairing is still to be established.

(4) What is the role of nematic quantum criticality in the phase diagram of the Fe-SCs? Because the fluctuations near a nematic quantum critical point may enhance (or create) superconductivity, and may also lead to anomalous metallic behaviour, it is tempting to view such a critical point near optimal doping as the key feature of the phase diagrams of the Fe-SCs. Evaluating this hypothesis is a key area for future work, and there are at least three reasons to view it with scepticism. First, nematicity in the Fe-SCs is largely coextensive with antiferromagnetism, which also appears to have a quantum phase transition near optimal doping. Electronic interactions mediated by long-range antiferromagnetic fluctuations can have similar effects to those of nematicity, although with important qualitative distinctions: antiferromagnetically mediated interactions are repulsive in some channels by virtue of their spin structure, and thus do not necessarily enhance superconductivity arising from other mechanisms, and the breaking of translation symmetry by antiferromagnetism confines non-Fermi-liquid behaviour to the vicinity of Fermi surface 'hot spots' connected by the ordering wave vector, at least in a perturbative regime. Second, because nematic order couples directly to strain, the nematicity itself is subject to long-range self-interactions arising from acoustic phonons[83]. These interactions essentially cut off the nematic fluctuations at sufficiently low energies, reducing any influence on superconductivity or metallic coherence. Finally, coupling to the lattice also makes nematicity highly sensitive to crystalline disorder, which may lead to non-perturbative effects such as a Griffith singularity near the quantum critical point[34,84]. Disentangling the effects of nematic fluctuations from those of magnetism, and evaluating the influence of the lattice and disorder on low-energy nematic fluctuations are therefore areas of great importance for future work, both theoretical and experimental. In this regard, Fe(Se,S) and Fe(Se,Te) are the model systems for such a study: they both host a pure nematic quantum critical point, yet superconductivity is enhanced in the latter but not in the former[46].

Overall, the Fe-SCs have emerged as an ideal material platform to study nematicity in crystalline solids. The ideas and tools developed in the context of Fe-SCs are already being used to shed light on other long-standing issues related to nematicity, and also to reveal nematicity in various old and new materials (for example, heavy fermion compounds and twisted bilayer graphene[85,86]). The Fe-SCs are also a perfect testbed to improve analytical and computation methods of condensed-matter theory. It is a tantalizing possibility that the study of their properties may shed light on the broader phenomenology of metallic quantum criticality, one of the most profound (and long unsolved) problems in quantum statistical mechanics. Clearly, it is the discovery of new materials that drives such advances. The past few years have witnessed an explosive discovery of diverse new candidates of nematic materials[87–90]. It is likely that our current understanding of electronic nematic phases is just the tip of the iceberg, and a discovery of completely new and unexpected facets is right around the corner.

References

1. Fradkin, E., Kivelson, S. A., Lawler, M. J., Eisenstein, J. P. & Mackenzie, A. P. Nematic Fermi fluids in condensed matter physics. *Annu. Rev. Condens. Matter Phys.* **1**, 153–178 (2010).
2. Lilly, M. P., Cooper, K. B., Eisenstein, J. P., Pfeiffer, L. N. & West, K. W. Evidence for an anisotropic state of two-dimensional electrons in high Landau levels. *Phys. Rev. Lett.* **82**, 394–397 (1999).
3. Borzi, R. A. et al. Formation of a nematic fluid at high fields in $Sr_3Ru_2O_7$. *Science* **315**, 214–217 (2007).

4. Lester, C. et al. Field-tunable spin-density-wave phases in $Sr_3Ru_2O_7$. *Nat. Mater.* **14**, 373–378 (2015).

5. Hinkov, V. et al. Electronic liquid crystal state in the high-temperature superconductor $YBa_2Cu_3O_{6.45}$. *Science* **319**, 597–600 (2008).

6. de la Cruz, C. et al. Magnetic order close to superconductivity in the iron-based layered $LaO_{1-x}F_xFeAs$ systems. *Nature* **453**, 899–902 (2008).

7. Nomura, T. et al. Crystallographic phase transition and high-T_c superconductivity in LaFeAsO:F. *Superconductor Sci. Technol.* **21**, 125028 (2008).

8. Fernandes, R. M. et al. Effects of nematic fluctuations on the elastic properties of iron arsenide superconductors. *Phys. Rev. Lett.* **105**, 157003 (2010).

9. Nandi, S. et al. Anomalous suppression of the orthorhombic lattice distortion in superconducting $Ba(Fe_{1-x}Co_x)_2 As_2$ single crystals. *Phys. Rev. Lett.* **104**, 057006 (2010).

10. Chu, J.-H., Kuo, H.-H., Analytis, J. G. & Fisher, I. R. Divergent nematic susceptibility in an iron arsenide superconductor. *Science* **337**, 710–712 (2012).

11. Chu, J.-H. et al. In-plane resistivity anisotropy in an underdoped iron arsenide superconductor. *Science* **329**, 824–826 (2010).

12. Dusza, A. et al. Anisotropic charge dynamics in detwinned $Ba(Fe_{1-x}Co_x)_2As_2$. *Europhys. Lett.* **93**, 37002 (2011).

13. Fu, M. et al. NMR search for the spin nematic state in a LaFeAsO single crystal. *Phys. Rev. Lett.* **109**, 247001 (2012).

14. Jiang, S., Jeevan, H. S., Dong, J. & Gegenwart, P. Thermopower as a sensitive probe of electronic nematicity in iron pnictides. *Phys. Rev. Lett.* **110**, 067001 (2013).

15. Chuang, T.-M. et al. Nematic Electronic Structure in the 'Parent' State of the Iron-Based Superconductor $Ca(Fe_{1-x}Co_x)_2As_2$. *Science* **327**, 181–184 (2010).

16. Lu, X. et al. Nematic spin correlations in the tetragonal state of uniaxial-strained $BaFe_{2-x}Ni_xAs_2$. *Science* **345**, 657–660 (2014).

17. Lu, X. et al. Spin-excitation anisotropy in the nematic state of detwinned FeSe. *Nat. Phys.* **18**, 806–812 (2021).

18. Kasahara, S. et al. Electronic nematicity above the structural and superconducting transition in $BaFe_2(As_{1-x}P_x)_2$. *Nature* **486**, 382–385 (2012).

19. Rosenthal, E. P. et al. Visualization of electron nematicity and unidirectional antiferroic fluctuations at high temperatures in NaFeAs. *Nat. Phys.* **10**, 225–232 (2014).

20. Wiecki, P. et al. NMR evidence for static local nematicity and its cooperative interplay with low-energy magnetic fluctuations in FeSe under pressure. *Phys. Rev. B* **96**, 180502 (2017).

21. Thewalt, E. et al. Imaging anomalous nematic order and strain in optimally doped $BaFe_2(As,P)_2$. *Phys. Rev. Lett.* **121**, 027001 (2018).

22. Shimojima, T. et al. Discovery of mesoscopic nematicity wave in iron-based superconductors. *Science* **373**, 1122–1125 (2021).

23. Lahiri, A., Klein, A. & Fernandes, R. M. Defect-induced electronic smectic state at the surface of nematic materials. *Phys. Rev. B* **106**, L140503 (2021).

24. Yi, M. et al. Symmetry-breaking orbital anisotropy observed for detwinned $Ba(Fe_{1-x}Co_x)_2As_2$ above the spin density wave transition. *Proc. Natl Acad. Sci. USA* **108**, 6878–6883 (2011).

25. Zhang, Y. et al. Symmetry breaking via orbital-dependent reconstruction of electronic structure in detwinned NaFeAs. *Phys. Rev. B* **85**, 085121 (2012).

26. Suzuki, Y. et al. Momentum-dependent sign inversion of orbital order in superconducting FeSe. *Phys. Rev. B* **92**, 205117 (2015).

27. Zhang, Y. et al. Distinctive orbital anisotropy observed in the nematic state of a FeSe thin film. *Phys. Rev. B* **94**, 115153 (2016).

28. Pfau, H. et al. Momentum dependence of the nematic order parameter in iron-based superconductors. *Phys. Rev. Lett.* **123**, 066402 (2019).

29. Watson, M. D. et al. Evidence for unidirectional nematic bond ordering in FeSe. *Phys. Rev. B* **94**, 201107 (2016).

30. Yi, M. et al. The nematic energy scale and the missing electron pocket in FeSe. *Phys. Rev. X* **9**, 041049 (2019).

31. Rhodes, L. C., Eschrig, M., Kim, T. K. & Watson, M. D. FeSe and the missing electron pocket problem. *Front. Phys.* **10**, 859017 (2022).

32. Yi, M. et al. Dynamic competition between spin–density wave order and superconductivity in underdoped $Ba_{1-x}K_xFe_2As_2$. *Nat. Commun.* **5**, 3711 (2014).

33. Tanatar, M. A. et al. Uniaxial-strain mechanical detwinning of $CaFe_2As_2$ and $BaFe_2As_2$ crystals: optical and transport study. *Phys. Rev. B* **81**, 184508 (2010).

34. Kuo, H.-H., Chu, J.-H., Palmstrom, J. C., Kivelson, S. A. & Fisher, I. R. Ubiquitous signatures of nematic quantum criticality in optimally doped Fe-based superconductors. *Science* **352**, 958–962 (2016).

35. Böhmer, A. E. et al. Nematic susceptibility of hole-doped and electron-doped $BaFe_2As_2$ iron-based superconductors from shear modulus measurements. *Phys. Rev. Lett.* **112**, 047001 (2014).

36. Böhmer, A. E. & Meingast, C. Electronic nematic susceptibility of iron-based superconductors. *Comptes Rendus Phys.* **17**, 90–112 (2016).

37. Gallais, Y. & Paul, I. Charge nematicity and electronic Raman scattering in iron-based superconductors. *Comptes Rendus Phys.* **17**, 113–139 (2016).

38. Chen, X., Maiti, S., Fernandes, R. M. & Hirschfeld, P. J. Nematicity and superconductivity: competition versus cooperation. *Phys. Rev. B* **102**, 184512 (2020).

39. Edelberg, D., Kumar, H., Shenoy, V., Ochoa, H. & Pasupathy, A. N. Tunable strain soliton networks confine electrons in van der Waals materials. *Nat. Phys.* **16**, 1097–1102 (2020).

40. Kissikov, T. et al. Uniaxial strain control of spin-polarization in multicomponent nematic order of $BaFe_2As_2$. *Nat. Commun.* **9**, 1058 (2018).

41. Caglieris, F. et al. Strain derivative of thermoelectric properties as a sensitive probe for nematicity. *npj Quantum Mater.* **6**, 27 (2021).

42. Sanchez, J. J. et al. The transport–structural correspondence across the nematic phase transition probed by elasto X-ray diffraction. *Nat. Mater.* **20**, 1519–1524 (2021).

43. Ikeda, M. S. et al. Elastocaloric signature of nematic fluctuations. *Proc. Natl Acad. Sci. USA* **118**, e2105911118 (2021).

44. Hosoi, S. et al. Nematic quantum critical point without magnetism in $FeSe_{1-x}S_x$ superconductors. *Proc. Natl Acad. Sci. USA* **113**, 8139–8143 (2016).

45. Hong, X. et al. Evolution of the nematic susceptibility in $LaFe_{1-x}Co_xAsO$. *Phys. Rev. Lett.* **125**, 067001 (2020).

46. Ishida, K. et al. Pure nematic quantum critical point accompanied by a superconducting dome. *Proc. Natl Acad. Sci. USA* **119**, e2110501119 (2022).

47. Worasaran, T. et al. Nematic quantum criticality in an Fe-based superconductor revealed by strain-tuning. *Science* **372**, 973–977 (2021).

48. Metzner, W., Rohe, D. & Andergassen, S. Soft Fermi surfaces and breakdown of Fermi-liquid behavior. *Phys. Rev. Lett.* **91**, 066402 (2003).

49. Lederer, S., Schattner, Y., Berg, E. & Kivelson, S. A. Enhancement of superconductivity near a nematic quantum critical point. *Phys. Rev. Lett.* **114**, 097001 (2015).

50. Yamase, H. & Zeyher, R. Superconductivity from orbital nematic fluctuations. *Phys. Rev. B* **88**, 180502 (2013).

51. Maier, T. A. & Scalapino, D. J. Pairing interaction near a nematic quantum critical point of a three-band CuO_2 model. *Phys. Rev. B* **90**, 174510 (2014).

52. Metlitski, M. A., Mross, D. F., Sachdev, S. & Senthil, T. Cooper pairing in non-Fermi liquids. *Phys. Rev. B* **91**, 115111 (2015).

53. Lederer, S., Schattner, Y., Berg, E. & Kivelson, S. A. Superconductivity and non-Fermi liquid behavior near a nematic quantum critical point. *Proc. Natl Acad. Sci. USA* **114**, 4905–4910 (2017).

54. Labat, D. & Paul, I. Pairing instability near a lattice-influenced nematic quantum critical point. *Phys. Rev. B* **96**, 195146 (2017).

55. Chubukov, A. V., Abanov, A., Wang, Y. & Wu, Y.-M. The interplay between superconductivity and non-Fermi liquid at a quantum-critical point in a metal. *Ann. Phys.* **417**, 168142 (2020).

56. Lawler, M. J., Barci, D. G., Fernández, V., Fradkin, E. & Oxman, L. Nonperturbative behavior of the quantum phase transition to a nematic Fermi fluid. *Phys. Rev. B* **73**, 085101 (2006).

57. Metlitski, M. A. & Sachdev, S. Quantum phase transitions of metals in two spatial dimensions. I. Ising-nematic order. *Phys. Rev. B* **82**, 075127 (2010).

58. Mross, D. F., McGreevy, J., Liu, H. & Senthil, T. Controlled expansion for certain non-Fermi-liquid metals. *Phys. Rev. B* **82**, 045121 (2010).

59. Lee, W.-C. & Phillips, P. W. Non-Fermi liquid due to orbital fluctuations in iron pnictide superconductors. *Phys. Rev. B* **86**, 245113 (2012).

60. Fitzpatrick, A. L., Kachru, S., Kaplan, J. & Raghu, S. Non-Fermi-liquid fixed point in a Wilsonian theory of quantum critical metals. *Phys. Rev. B* **88**, 125116 (2013).

61. Dalidovich, D. & Lee, S.-S. Perturbative non-Fermi liquids from dimensional regularization. *Phys. Rev. B* **88**, 245106 (2013).

62. Shibauchi, T., Carrington, A. & Matsuda, Y. A quantum critical point lying beneath the superconducting dome in iron pnictides. *Annu. Rev. Condens. Matter Phys.* **5**, 113–135 (2014).

63. Analytis, J. G. et al. Transport near a quantum critical point in $BaFe_2(As_{1-x}P_x)_2$. *Nat. Phys.* **10**, 194–197 (2014).

64. Licciardello, S. et al. Electrical resistivity across a nematic quantum critical point. *Nature* **567**, 213–217 (2019).

65. Shimojima, T. et al. Ultrafast nematic-orbital excitation in FeSe. *Nat. Commun.* **10**, 1946 (2019).

66. Fang, C., Yao, H., Tsai, W.-F., Hu, J. & Kivelson, S. A. Theory of electron nematic order in LaFeAsO. *Phys. Rev. B* **77**, 224509 (2008).

67. Baek, S.-H. et al. Orbital-driven nematicity in FeSe. *Nat. Mater.* **14**, 210–214 (2015).

68. Wang, Q. et al. Strong interplay between stripe spin fluctuations, nematicity and superconductivity in FeSe. *Nat. Mater.* **15**, 159–163 (2016).

69. Böhmer, A. E. & Kreisel, A. Nematicity, magnetism and superconductivity in FeSe. *J. Phys. Condens. Matter* **30**, 023001 (2018).

70. Lee, C.-C., Yin, W.-G. & Ku, W. Ferro-orbital order and strong magnetic anisotropy in the parent compounds of iron-pnictide superconductors. *Phys. Rev. Lett.* **103**, 267001 (2009).

71. Onari, S. & Kontani, H. Self-consistent vertex correction analysis for iron-based superconductors: mechanism of coulomb interaction-driven orbital fluctuations. *Phys. Rev. Lett.* **109**, 137001 (2012).

72. Gastiasoro, M. N., Paul, I., Wang, Y., Hirschfeld, P. J. & Andersen, B. M. Emergent defect states as a source of resistivity anisotropy in the nematic phase of iron pnictides. *Phys. Rev. Lett.* **113**, 127001 (2014).

73. Fernandes, R. M., Abrahams, E. & Schmalian, J. Anisotropic in-plane resistivity in the nematic phase of the iron pnictides. *Phys. Rev. Lett.* **107**, 217002 (2011).

74. Valenzuela, B., Bascones, E. & Calderón, M. J. Conductivity anisotropy in the antiferromagnetic state of iron pnictides. *Phys. Rev. Lett.* **105**, 207202 (2010).

75. de Carvalho, V. S. & Fernandes, R. M. Resistivity near a nematic quantum critical point: impact of acoustic phonons. *Phys. Rev. B* **100**, 115103 (2019).

76. Kuo, H. & Fisher, I. R. Effect of disorder on the resistivity anisotropy near the electronic nematic phase transition in pure and electron-doped $BaFe_2As_2$. *Phys. Rev. Lett.* **112**, 227001 (2014).

77. Tanatar, M. A. et al. Origin of the resistivity anisotropy in the nematic phase of FeSe. *Phys. Rev. Lett.* **117**, 127001 (2016).

78. Mirri, C. et al. Origin of the resistive anisotropy in the electronic nematic phase of $BaFe_2As_2$ revealed by optical spectroscopy. *Phys. Rev. Lett.* **115**, 107001 (2015).

79. Malinowski, P. et al. Suppression of superconductivity by anisotropic strain near a nematic quantum critical point. *Nat. Phys.* **16**, 1189–1193 (2020).

80. Wang, L. et al. Superconductivity-enhanced nematicity and 's + d' gap symmetry in $Fe(Se_{1-x}S_x)$. *Phys. Status Solidi b* **254**, 1600153 (2017).

81. Sprau, P. O. et al. Discovery of orbital-selective Cooper pairing in FeSe. *Science* **357**, 75–80 (2017).

82. Hanaguri, T. et al. Two distinct superconducting pairing states divided by the nematic end point in $FeSe_{1-x}S_x$. *Sci. Adv.* **4**, eaar6419 (2018).

83. Paul, I. & Garst, M. Lattice effects on nematic quantum criticality in metals. *Phys. Rev. Lett.* **118**, 227601 (2017).

84. Reiss, P., Graf, D., Haghighirad, A. A., Vojta, T. & Coldea, A. I. Signatures of a quantum Griffiths phase close to an electronic nematic quantum phase transition. *Phys. Rev. Lett.* **127**, 246402 (2021).

85. Rosenberg, E. W., Chu, J.-H., Ruff, J. P. C., Hristov, A. T. & Fisher, I. R. Divergence of the quadrupole-strain susceptibility of the electronic nematic system $YbRu_2Ge_2$. *Proc. Natl Acad. Sci. USA* **116**, 7232–7237 (2019).

86. Cao, Y. et al. Nematicity and competing orders in superconducting magic-angle graphene. *Science* **372**, 264–271 (2021).

87. Yonezawa, S. Nematic superconductivity in doped Bi_2Se_3 topological superconductors. *Condens. Matter* **4**, 2 (2019).

88. Kohama, Y. et al. Possible observation of quantum spin-nematic phase in a frustrated magnet. *Proc. Natl Acad. Sci. USA* **116**, 10686–10690 (2019).

89. Seo, S. et al. Nematic state in $CeAuSb_2$. *Phys. Rev. X* **10**, 011035 (2020).

90. Eckberg, C. et al. Sixfold enhancement of superconductivity in a tunable electronic nematic system. *Nat. Phys.* **16**, 346–350 (2020).

91. Chibani, S. et al. Lattice-shifted nematic quantum critical point in $FeSe_{1-x}S_x$. *npj Quantum Mater.* **6**, 37 (2020).

Acknowledgements

Competing interests

The authors declare no competing interests.

Additional information

Correspondence should be addressed to Anna E. Böhmer.